Research Square

Preprints are preliminary reports that have not undergone peer review.
They should not be considered conclusive, used to inform clinical practice,
or referenced by the media as validated information.

Sex-specific white adipose tissue dysfunction in the TDP-43 A315T mice model of amyotrophic lateral sclerosis (ALS)

Cristina Benito-Casado
Universidad CEU-San Pablo, CEU Universities
Águeda Ferrer-Donato
Universidad CEU-San Pablo, CEU Universities
Esther Durán-Mateos
Universidad CEU-San Pablo, CEU Universities
Carmen M. Fernandez-Martos
Carmen.fernandezmartos@ceu.es

Universidad CEU-San Pablo, CEU Universities

Research Article

Keywords: Amyotrophic lateral sclerosis (ALS), TAR DNA binding protein (TDP-43), White adipose tissue (WAT), leptin, metabolic dysfunction, sex differences

Posted Date: November 7th, 2026

DOI: https://doi.org/10.21203/rs.3.rs-9925200/v1

License: This work is licensed under a Creative Commons Attribution 4.0 International License.
Read Full License

Additional Declarations: No competing interests reported.

Abstract

Sex differences in the metabolic regulation of energy homeostasis are increasingly recognized as modifiers of amyotrophic lateral sclerosis (ALS) progression; however, their impact on adipose tissue pathology remains insufficiently characterized. White adipose tissue (WAT), beyond its role in triglyceride storage, functions as an endocrine organ and is the primary source of leptin, a key adipokine regulating neuroendocrine and metabolic pathways. In ALS, circulating leptin levels are altered in both patients and animal models and correlate with adiposity and disease progression. In parallel, leptin signaling pathways are disrupted in ALS mouse models. Whether these alterations, particularly in a sex-dependent manner, reflect a primary dysfunction of WAT during disease progression remains unclear. Here, we characterize WAT remodeling in female TDP-43^{A315T} mice across disease stages using histological and molecular analyses combined with plasma leptin measurements. Female TDP-43^{A315T} mice exhibited progressive WAT impairments, including adipocyte atrophy, structural disorganization, and altered circulating leptin levels. These changes were associated with transcriptional alterations in key genes regulating adipocyte differentiation, thermogenesis, and TDP-43 homeostasis, consistent with impaired adipose tissue plasticity. Notably, WAT alterations emerged later than previously reported in males, indicating sex-specific temporal dynamics. In parallel, hypothalamic gene expression analyses revealed increased orexigenic signaling despite relatively preserved circulating leptin levels, suggesting early central leptin dysregulation. Together, these findings support the existence of sex-dependent mechanisms affecting both peripheral adipose tissue remodeling and central metabolic regulation in ALS. This study identifies WAT as a relevant peripheral contributor to metabolic dysfunction and highlights leptin-related pathways as potential targets for sex-specific therapeutic strategies.

1. INTRODUCTION

Amyotrophic lateral sclerosis (ALS) is a fatal neurodegenerative disorder characterized by progressive motor neuron degeneration and accompanied by systemic metabolic alterations (Al-Khayri et al., 2024). Beyond its classical motor manifestations, ALS is increasingly recognized as a multisystem disease in which disrupted energy homeostasis plays a central role. Hypermetabolism is a consistent clinical feature associated with accelerated disease progression and reduced survival (Rosina et al., 2025; Steyn et al., 2018). However, the underlying mechanisms driving this metabolic imbalance remain poorly understood.

Adipose tissue is a metabolically active organ that plays a key role in systemic energy balance. White adipose tissue (WAT) regulates energy storage and endocrine signaling, while brown adipose tissue dissipates energy through thermogenesis. WAT functions as an endocrine organ by secreting adipokines such as leptin, which links peripheral metabolic status to neuroendocrine and immune pathways (Sabaratnam, 2025). In ALS, patients frequently present dyslipidaemia and altered adipokine profiles, including leptin (Rosina et al., 2025). Experimental studies using transgenic (Tg) superoxide dismutase 1 (SOD1) mouse models have demonstrated an early contribution of adipose tissue to disease progression (Martin & Wong, 2020; Thompson et al., 2025). In particular, the loss of adipose depots and

metabolic alterations precede overt neuromuscular decline (Martin & Wong, 2020; Thompson et al., 2025).

We and others have identified WAT alterations in TDP-43-based models, which are relevant given that TDP-43 pathology is present in approximately 97% of ALS cases (Chen-Plotkin et al., 2010). In male TDP-43^{A315T} mice, early adipose tissue remodeling, including adipocyte atrophy and inflammatory infiltration has been described (Benito-Casado, et al., 2025a). Emerging data from rNLS8 mice, an inducible Tg model of TDP-43 (Walker et al., 2015), further suggest sex-dependent alterations in leptin-related pathways across peripheral tissues and the central nervous system (CNS) (Benito-Casado, et al., 2025b), indicating that metabolic dysregulation in ALS may be modulated by biological sex.

Leptin signaling, primarily mediated through ObRb receptor and activation of Janus tyrosine kinase/signal transducer and activator of transcription (JAK/STAT) and phosphatidylinositol 3-kinase (PI3K)/Akt pathways, plays a crucial role in metabolic regulation and has been implicated in neuroprotection and neuroinflammation (Evans et al., 2021). Alterations in these pathways have been reported in ALS models, including $SOD1^{G93A}$ and TDP-43^{A315T} mice (Ferrer-Donato et al., 2021; Picher-Martel et al., 2023). Importantly, circulating leptin levels differ between sexes, with women typically showing higher concentrations (Benito-Casado, et al., 2025a; Picher-Martel et al., 2023), suggesting potential sex-specific regulation of adipose and central metabolic pathways. While this difference may confer a degree of metabolic resilience, clinical data indicate that women with ALS often experience faster motor decline despite longer overall survival (Grassano et al., 2024), highlighting the complexity of sex-dependent interactions between metabolism, disease progression and neurodegeneration.

In this context, we investigated WAT remodeling in female TDP-43^{A315T} mice together with hypothalamic leptin-related signaling to characterize sex-dependent metabolic alterations throughout disease progression. Based on the sex-specific alterations reported in ALS and our previous observations in male TDP-43^{A315T} mice (Ferrer-Donato et al., 2021; Benito-Casado, et al., 2025a), we hypothesized that female mice would exhibit WAT remodeling and alterations in hypothalamic leptin-related signaling, albeit with a distinct temporal profile. To test this hypothesis, we combined histological and molecular approaches to assess WAT pathology and central and peripheral regulators of energy homeostasis at different stages of disease progression. Our findings demonstrate that WAT pathology is also present in female mice but evolves according to a temporal pattern distinct from that observed in males, supporting the existence of sex-specific mechanisms underlying metabolic dysfunction in ALS.

2. MATERIALS AND METHODS

2.1 Experimental Animals

Two cohorts of age- and sex-matched TDP-43^{A315T} Tg mice (Wegorzewska et al., 2009, JAX stock #010700) and WT non-Tg littermates (C57Bl/6) (n = 60/genotype) were included in this study. For each genotype, 15 animals were allocated for histological analyses and 15 for molecular biology experiments.

In both cases, the ALS-like disease was categorized into three stages (n = 5/stage): 1) asymptomatic (approximately 42–45 days (d) of age), 2) onset (approximately 65–70 d), and 3) end-stage (approximately 95–100 ± 2 d). Disease stages were defined according to the clinical progression observed in male TDP-43^{A315T} mice to ensure consistency and avoid ambiguity arising from reported sex-related differences in mean survival time in this ALS model (Hatzipetros et al., 2014; Wegorzewska et al., 2009). This approach allowed the evaluation of females at equivalent chronological age rather than disease stages, ensuring alignment with the timepoints analysed in males and enabling direct sex-based comparisons. Animals were euthanized separately at each defined disease stage in independent cohorts. Female mice expressing the human TDP-43 (hTDP-43) transgene were confirmed via PCR following the distributor's protocol (JAX protocol 26362). All procedures involving animal care and use were approved by the Animal Ethics Committee of the Hospital Nacional de Parapléjicos, Toledo (Spain) (Approval No. 26/OH 2018), in accordance with the Spanish Guidelines for the Care and Use of Animals for Scientific Purposes. All analyses were performed by personnel blinded to the animal genotype.

2.2 Perfusion and tissue collection

All mice were terminally anesthetized by intraperitoneal injection of sodium pentobarbitone (140 mg/kg) and transcardially perfused with 0.01 M phosphate-buffered saline (PBS; pH 7.4) at room temperature (RT). All procedures were performed during the midpoint of the light phase (between 11:00 AM and 1:00 PM) to minimize circadian variability. Blood samples were collected and processed as previously described (Rodriguez et al., 2021). Both scWAT and pgWAT tissues, as well as the hypothalamus, were carefully dissected and processed for histological and/or molecular biology analyses. For molecular studies, pgWAT samples were divided into two fractions, immediately frozen on dry ice, and stored at -80 ºC until further processing. These samples were subsequently processed independently for quantitative real-time PCR (RT-qPCR) and Western blot (WB) analyses. Hypothalamic samples were immediately frozen on dry ice, stored at -80 ºC, and later processed for RT-qPCR analysis. For histological analysis, scWAT and pgWAT samples were rinsed in PBS, post-fixed in 70% ethanol, and stored at 4 ºC until paraffin embedding using an automatic tissue processor (ATP 1000, Histo-line, Italy). Paraffin-embedded sections (4 µm thick) were cut using a microtome (Leica Biosystems, Mannheim, Germany).

2.3 Immunohistochemical (IHC) analysis

IHC analyses were performed following previously published and validated protocols for adipose tissue characterization, as described in detail by (Benito-Casado, et al., 2025a). Both scWAT and pgWAT samples were processed, sectioned, and stained using standardized procedures to ensure reproducibility and inter-sample comparability, in line with established adipose tissue histopathology methodologies (Cancello et al., 2006; Cinti et al., 2005).

Digital photomicrographs were acquired using a Leica CTR 6000 microscope (Leica Microsystems, Mannheim, Germany). Quantitative analyses were conducted on images captured at 20× magnification, while semiquantitative histopathological assessments were performed on images obtained at 10× magnification, as commonly applied in the evaluation of adipose tissue inflammation, vascularization,

and remodeling (Cancello et al., 2006; Sun et al., 2013). For each sample, ten randomly selected, non-overlapping fields from anatomically distinct regions were analysed to account for intratissue heterogeneity, a critical feature of WAT architecture (Parlee et al., 2014) (total number of analysed fields: n = 60).

Image analysis was performed using ImageJ software (NIH, Bethesda, MD, USA; https://imagej.net/ij/). Regions of interest were manually delineated, and all sections were evaluated using uniform and predefined morphological criteria. Crown-like structures (CLSs), defined as macrophage aggregates surrounding dead or dying adipocytes, were identified and quantified as a hallmark of adipose tissue inflammation, according to previously established definitions (Cancello et al., 2006; Cinti et al., 2005). Blood vessels (BV) were also identified and quantified based on standard morphological criteria (Sun et al., 2013). Inflammatory and degenerative features, including mononuclear cell infiltration, fibrotic remodeling, and necrotic alterations, such as disruption of adipocyte membrane integrity and loss of normal tissue architecture, were assessed using a semiquantitative scoring system adapted from established adipose tissue pathology protocols (Cancello et al., 2006; Sun et al., 2013) and as previously applied in our own work (Benito-Casado, et al., 2025a). Normal adipocytes were defined as cells displaying a well-defined spherical or polygonal morphology with a continuous cytoplasmic membrane and no visible membrane disruptions.

2.4 RNA isolation and RT-qPCR analysis

Total RNA was extracted from pgWAT and hypothalamus using the RNeasy Mini Kit (Qiagen, Cat. No. 1023539), according to the manufacturer's instructions. RNA concentration and purity were assessed spectrophotometrically prior to downstream applications. Complementary DNA (cDNA) was synthesized from 0.5 µg of total RNA. Relative mRNA expression levels of CCAAT/enhancer-binding protein β (*C/EBPβ*), peroxisome proliferator-activated receptor gamma (*PPARγ*), mitochondrial uncoupling protein 1 (*UCP1*), and TAR DNA-binding protein 43 (*TDP-43*) were determined in pgWAT as previously described (Benito-Casado, et al., 2025a). Relative mRNA expression levels of the long isoform of the leptin receptor (*ObRb*), agouti-related peptide (*AgRP*), and pro-opiomelanocortin (*POMC*) were determined in the hypothalamus as previously described (Rodríguez-Sánchez et al., 2022). Neuropeptide Y (*NPY*) expression was assessed using newly designed primer pairs. Primer sequences for all genes analysed are presented in Table 1. qPCR was performed using a CFX96 Real-Time PCR Detection System and CFX Manager 3.0 software (Bio-Rad), following the manufacturer's recommendations. All samples were run in duplicate. Gene expression levels were normalized to the housekeeping genes *Actb* and *18S* (Fernandez et al., 2010; González-Fernández et al., 2014). Relative gene expression was calculated using the comparative ΔΔCt method (Livak & Schmittgen, 2001).

Table 1
List of RT-qPCR primers.

Gene	Forward primer	Reverse primer	Acc no.
C/EBPβ	5'-GACAAGCTGAGCGACGAGT-3'	5'-CGCACCGCGATGTTGTTG-3'	NM_001287738
PPARγ	5'-AGAGGTGGCCATCCGAATTT-3'	5'-ACGGCTTCTACGGATCGAAA-3'	NM_011146
UCP-1	5'-GGCCTCTACGACTCAGTCCA-3'	5'-TAAGCCGGCTGAGATCTTGT-3'	NM_009463
TDP-43	5'-GGGCGATGGTGTGACTGTAA-3'	5'-GCTCGTCTGGGCTTTGCTTA-3'	NM_145556
ObRb	5'-CCCCCACTGAAAGACAGCTT-3'	5'-TTCACATCCCCGAAGACTGC-3'	NM_146146.
AgRP	5'-TGGCCTCAAGAAGACAACTG-3'	5'-CATTGGCTAGGTGCGACTAC-3'	NM_007427
POMC	5'-AGAACGCCATCATCAAGAAC-3'	5'-AAGAGGCTAGAGGTCATCAG-3'	NM_008895
NPY	5'-GTGGATCTCTTCTCTCACAGAGG-3'	5'-GCCCAAACACACGAGCAGAG-3'	NM_023456
β-actin	5'-AAGTCCCTCACCCTCCCAAAAG-3'	5'-AAGCAATGCTGTCACCTTCCC-3'	NM_007393.3
18S	5'-AGTCCCTGCCCTTTGTACACA-3'	5'-GCCTCACTAAACCATCCAATCG-3'	NR_003278

Primers used for RT-qPCR analysis of the genes assessed here, including the gene symbol, primer sequence (forward and reverse sequence respectively) and GenBank accession number.

2.5 Protein extraction and WB analysis

Proteins were isolated from pgWAT using RIPA lysis buffer (Santa Cruz Biotechnology, Cat. No. sc-24948), according to the manufacturer's instructions. Protein concentration was determined prior to electrophoresis. Equal amounts of denatured protein (20 μg) were separated on Bolt® Bis-Tris Plus gels (Invitrogen, Cat. No. NW04120BOX) and subsequently transferred onto polyvinylidene difluoride (PVDF) membranes (Bio-Rad, Cat. No. 1620177). Membranes were blocked and incubated overnight at 4 ºC with a rabbit anti-TDP-43 primary antibody (1:1000; Proteintech, Cat. No. 10782-2-AP). After washing, membranes were incubated with an HRP-conjugated anti-rabbit secondary antibody (Vector Laboratories, Cat. No. PI-1000), as previously described (Ferrer-Donato et al., 2021). Immunoreactive bands were visualized using standard chemiluminescent detection methods. A mouse anti-β-actin antibody (1:1000; Santa Cruz Biotechnology, Cat. No. sc-47778) was used as a loading control to ensure equal protein loading across samples.

2.6 Measurement of plasma leptin by enzyme-linked immunosorbent assay (ELISA)

Plasma leptin concentrations were measured using an ELISA according to the manufacturer's instructions. Leptin levels were determined using the Leptin (Mouse/Rat) ELISA Kit (Phoenix Pharmaceuticals, Inc., Cat. No. EK-003-17). Plasma samples were diluted 1:5 and assayed in duplicate. The assay sensitivity was 62.5 pg/mL, with an upper limit of quantification of 4000 pg/mL. The intra-assay and inter-assay coefficients of variation (CVs) were < 10% and < 15%, respectively, as provided by the manufacturer.

2.7 Statistical analysis

Statistical analyses were performed using GraphPad Prism software (version 10.2.0). Outliers were identified and removed using the ROUT method (Q = 1%). Normal distribution and variance homogeneity were assessed by means of the Shapiro-Wilk normality test. For IHC analyses, comparisons between groups were performed using the Mann-Whitney U test, given the non-parametric nature of the data. Molecular biology data were analysed using a two-way analysis of variance (ANOVA) without repeated measures, followed by Dunnett's post hoc test for comparisons of all experimental groups against WT mice at 42 d, and Tukey's post hoc test for multiple pairwise comparisons between all groups when appropriate. Within-group comparisons were conducted using unpaired Student's t-test for normally distributed data or the Mann-Whitney U test for non-normally distributed data. Data are presented as mean ± standard error of the mean (SEM). Differences were considered statistically significant at $p < 0.05$.

3. RESULTS

3.1 Female TDP-43^{A315T} mice display early and progressive histopathological remodeling of WAT

Previous work from our group demonstrated that male TDP-43^{A315T} mice exhibit marked histopathological alterations in WAT from early presymptomatic stages. However, the status of WAT during disease progression in female TDP-43^{A315T} mice had not been characterized. To address this, we performed a comprehensive histological analysis of scWAT and pgWAT in female TDP-43^{A315T} mice at 42, 60 and 95 d of age, corresponding to presymptomatic, early symptomatic and advanced stages of disease, respectively, and compared them with age-matched WT littermates.

Histological evaluation of H&S-stained sections revealed significant alterations in both WAT depots across disease stages (Figs. 1–3). Quantitative analysis showed a significant reduction in the number of BV in scWAT at 42 d (Fig. 1b; $p = 0.042$) and in pgWAT at 95 d of age (Fig. 3b; $p = 0.001$) in female TDP-43^{A315T} mice compared with WT controls. In parallel, CLSs, a histological hallmark of adipose tissue inflammation, were significantly increased in scWAT at 60 d (Fig. 2c; $p < 0.001$) and in pgWAT at 95 d

(Fig. 3c; $p < 0.001$) in female TDP-43^{A315T} mice. CLSs were not detected at 42 d of age in either genotype.

Beyond these parameters, a detailed semi-quantitative assessment revealed widespread structural alterations in WAT depots of female TDP-43^{A315T} mice (Figs. 1c, 2d and 3d). IHC analysis demonstrated a marked increase in mononuclear cell infiltrate in both scWAT and pgWAT at all analysed stages compared with age-matched female WT littermates (Figs. 1d, 2e and 3e; $p < 0.001$ for all comparisons). In addition, overall tissue integrity was significantly compromised in scWAT and pgWAT across all disease stages, with female TDP-43^{A315T} mice showing lower integrity scores compared with WT controls at 42 (Fig. 1e; $p < 0.001$ for both depots), 60 (Fig. 2f; $p < 0.001$ for scWAT and $p = 0.002$ for pgWAT) and 95 d of age (Fig. 3f; $p < 0.001$ for both depots). Consistently, a significant reduction in the proportion of adipocytes displaying a normal membrane morphology was observed in both depots at 42, 60 and 95 d of age in female TDP-43^{A315T} mice (Figs. 1f, 2g and 3g; $p < 0.001$ for all comparisons). Finally, fibrotic remodeling was detected exclusively in scWAT at the advanced disease stage, with female TDP-43^{A315T} mice at 95 d exhibiting significantly increased fibrosis compared with WT littermates (Fig. 3h; $p < 0.001$).

3.2 Altered expression of adipogenic and thermogenic genes in pgWAT of female TDP-43^{A315T} mice

To determine whether the histopathological alterations observed in WAT were accompanied by molecular changes, we performed qPCR analysis on pgWAT samples collected across disease stages. pgWAT depot was selected due to its high metabolic activity and its established role in systemic energy homeostasis and metabolic inflammation, particularly as a representative visceral adipose tissue in rodent models (Chavakis et al., 2023; Zwick et al., 2018).

qPCR analysis of key adipogenic transcription factors revealed a dynamic and stage-dependent dysregulation in female TDP-43^{A315T} mice. Relative mRNA expression of *C/EBPβ* was significantly reduced at 42 d of age compared with WT littermates (Fig. 4a; $p = 0.025$). In contrast, at 60 d of age, *C/EBPβ* expression was markedly increased in female TDP-43^{A315T} mice compared with both age-matched WT controls ($p < 0.001$) and TDP-43^{A315T} mice at 42 d ($p = 0.02$). At 95 d, *C/EBPβ* expression significantly declined compared with levels at both 42 ($p = 0.002$) and 60 d ($p < 0.001$) (Fig. 4a). With respect to *PPARγ*, at 60 d, mRNA levels in female TDP-43^{A315T} mice showed a significant reduction compared with WT controls (Fig. 4b; $p = 0.060$). At 95 d, *PPARγ* expression was significantly decreased in female TDP-43^{A315T} mice compared with both age-matched WT littermates ($p < 0.001$) and TDP-43^{A315T} mice at 60 d ($p = 0.003$).

Furthermore, to assess potential activation of thermogenic pathways, the expression of *UCP1* was analysed. qPCR revealed a significant increase in *UCP1* mRNA levels in pgWAT of female TDP-43^{A315T} mice at 60 d compared with WT controls (Fig. 4c; $p < 0.001$). *UCP1* expression at 60 d was also

significantly higher than that observed at both 42 and 95 d in female TDP-43^{A315T} mice ($p < 0.001$ for both comparisons).

3.3 Increased TDP-43 expression in pgWAT of female TDP-43^{A315T} mice

To investigate whether alterations in key adipogenic and thermogenic gene expression profiles were associated with changes in TDP-43 regulation within adipose tissue, endogenous murine TDP-43 (*mTDP-43*) expression was analysed in pgWAT. qPCR analysis demonstrated a significant upregulation of *mTDP-43* mRNA levels in female TDP-43^{A315T} mice at 42 d compared with WT littermates (Fig. 4d; $p = 0.034$). Consistent with transcript-level changes, WB analysis revealed a qualitatively consistently stronger TDP-43 protein signal in pgWAT from female TDP-43^{A315T} mice compared with WT controls at all analysed stages (Fig. 4e–g; Supplementary Fig. 1). These findings parallel those previously described in male TDP-43^{A315T} mice.

3.4 Plasma leptin levels in female TDP-43^{A315T} mice

Since the molecular alterations identified in the pgWAT of female TDP-43^{A315T} mice involved pathways related to adipocyte function and given that WAT is the primary source of leptin, we sought to determine whether these changes were reflected at the systemic level by alterations in plasma leptin concentrations. Previous studies in male TDP-43^{A315T} mice have reported a pronounced reduction in circulating leptin levels during disease progression. To assess whether female TDP-43^{A315T} mice exhibited a similar pattern, plasma leptin concentrations were measured by ELISA at 42, 60, and 95 d of age. Female TDP-43^{A315T} mice showed higher plasma leptin levels at 60 and 95 d compared with age-matched WT littermates; however, these differences did not reach statistical significance (Fig. 5). In contrast, female WT mice exhibited a significant decline in plasma leptin levels at 95 d compared with WT mice at 42 ($p = 0.032$) and 60 d ($p = 0.026$) (Fig. 5).

3.5 Altered hypothalamic leptin ObRb receptor and orexigenic neuropeptide expression in female TDP-43^{A315T} mice

Given the central role of leptin in hypothalamic regulation of energy balance, plasma leptin levels quantified by ELISA were examined in parallel with its ObRb receptors and hypothalamic gene expression, even in the absence of significant differences between genotypes. Relative mRNA expression of *ObRb* was significantly increased in female TDP-43^{A315T} mice at 42 d of age compared with WT littermates (Fig. 6a; $p = 0.031$). Relative mRNA expression of *NPY* was also significantly increased in female TDP-43^{A315T} at 42 d compared with WT littermates (Fig. 6b; $p = 0.042$). For *AgRP*, relative mRNA expression was significantly increased in female TDP-43^{A315T} at 42 d compared with WT littermates too (Fig. 6c; $p = 0.043$). *AgRP* expression was significantly higher in female TDP-43^{A315T} at 60

d compared with TDP-43^{A315T} mice at 95 d of age (p = 0.008). No significant changes in the relative expression of *POMC* were observed (Fig. 6d).

4. DISCUSSION

ALS is increasingly recognized as a multisystem disorder in which neurodegeneration extends beyond the motor system and is accompanied by systemic metabolic alterations, including impaired energy balance and dysregulation of adipokines such as leptin (Ahmed et al., 2019; Benito-Casado, et al., 2025a; Picher-Martel et al., 2023). Within this context, WAT represents a relevant peripheral organ linking metabolic and inflammatory processes with disease progression. Building on previous findings demonstrating early adipose tissue alterations in male TDP-43^{A315T} mice (Benito-Casado, et al., 2025a), the present study provides the first longitudinal characterization of WAT remodeling in female TDP-43^{A315T} mice, allowing assessment of sex-dependent differences across disease stages.

At the presymptomatic stage, female TDP-43^{A315T} mice already exhibited evidence of WAT remodeling and tissue damage. These structural changes coincided with a significant upregulation of endogenous *mTDP-43* mRNA in pgWAT, suggesting that transcriptional TDP-43 dysregulation in WAT is an early event in female TDP-43^{A315T} mice. The simultaneous appearance of inflammatory remodeling and increased *mTDP-43* mRNA expression is consistent with an initial stress-associated phase in WAT, characterized by immune cell recruitment and early architectural disruption. Notably, CLSs were absent at this stage (Benito-Casado, et al., 2025a), and the overall severity of alterations was milder than that previously reported in male TDP-43^{A315T} mice, indicating that although WAT is an early target in both sexes in TDP-43^{A315T} mice, the early pathological response differs quantitatively and qualitatively between males and females.

As disease progressed to 60 d of age, WAT pathology in female TDP-43^{A315T} mice became more prominent. The observed histological and molecular alterations suggest the establishment of a pro-inflammatory adipose environment accompanied by alteration in pathways regulating adipocyte differentiation and metabolic activity. Given the established role of C/EBPβ in promoting inflammatory gene programs and limiting full PPARγ activation in adipocytes and macrophages (Guilherme et al., 2009; Ito et al., 2009), this transcriptional profile aligns closely with inflammation-linked adipose remodeling. The concomitant increase in *UCP1* mRNA expression levels suggests activation of thermogenic pathways, consistent with increased energy expenditure and metabolic stress, processes that have been implicated in ALS-associated hypermetabolism (Herz & Kiefer, 2019; Ikeda & Yamada, 2020). Importantly, these molecular changes were not observed in male TDP-43^{A315T} mice at equivalent stages (Benito-Casado, et al., 2025a), highlighting fundamentally distinct sex-specific molecular responses within adipose tissue.

By the advanced disease stage, female TDP-43^{A315T} mice exhibited widespread WAT degeneration, with alterations in BV density and increased CLSs now evident in pgWAT, together with persistent

mononuclear infiltration and adipocyte necrosis in both WAT depots. Fibrotic remodeling, however, emerged only at this late stage and was restricted to scWAT, in contrast to male TDP-43^{A315T} mice in which fibrosis was detected earlier during disease progression (Benito-Casado, et al., 2025a). Integrating histological and molecular data across disease stages suggests that WAT pathology in females does not simply represent a delayed version of the male phenotype but follows a distinct temporal trajectory characterized by early inflammatory stress, mid-stage transcriptional reprogramming and late-stage structural collapse and fibrosis. Whether this reflects intrinsic sex-dependent differences in inflammatory regulation, depot-specific vulnerability or responses to TDP-43 accumulation remains to be clarified and will require inclusion of additional intermediate time points and mechanistic analyses.

In parallel with structural and molecular differences in WAT remodeling, plasma leptin dynamics also differed between sexes. Unlike male TDP-43^{A315T} mice, which display a marked decline in circulating leptin levels during disease progression (Ferrer-Donato et al., 2021), female TDP-43^{A315T} mice tended to preserve leptin concentrations. Interestingly, WT females exhibited an age-associated decline in plasma leptin that was not observed in TDP-43^{A315T} mice, suggesting altered regulation of leptin secretion or turnover in the disease context. This age-dependent reduction in circulating leptin is consistent with previous studies reporting an inverse relationship between leptin levels and age, even after adjusting for adiposity, particularly in females, and likely reflects the combined effects of endocrine changes, including reduced estrogen signalling, and age-related alterations in adipose tissue function (Becerril et al., 2022; Isidori et al., 2000). The absence of this decline in TDP-43^{A315T} females may therefore indicate a disruption of the physiological mechanisms governing leptin homeostasis. In line with this, ALS models, including TDP-43^{A315T} mice, exhibit early and progressive dysfunction of WAT as well as systemic metabolic alterations such as hypermetabolism and energy imbalance, which can uncouple circulating leptin levels from adipose mass and age-related regulation (Benito-Casado, et al., 2025a; Ferrer-Donato et al., 2021).

Moreover, these peripheral alterations occurred in parallel with early changes in hypothalamic leptin-responsive pathways, including increased expression of the *ObRb* receptor and the orexigenic neuropeptides *NPY* and *AgRP*, key neuronal targets of leptin signaling in the arcuate nucleus of the hypothalamus that regulate energy intake and expenditure (Morselli et al., 2018). This apparent dissociation between circulating leptin levels and hypothalamic signaling suggests an early dysregulation of central leptin responsiveness, consistent with emerging evidence that hypothalamic dysfunction contributes to metabolic impairment and disease progression in ALS (Rosina et al., 2025). Given leptin's central roles in energy homeostasis, these observations support the existence of a dysregulated adipose-brain axis linking peripheral adipose tissue remodeling with altered hypothalamic control of energy balance (Caron et al., 2018), a bidirectional system critical for maintaining metabolic homeostasis. Such alterations may reflect compensatory mechanisms aimed at preserving metabolic balance or modulating inflammatory responses during ALS progression and could contribute to the sex-specific differences observed in disease trajectory.

Together, this study identifies WAT as a sex-sensitive peripheral target of TDP-43-associated pathology in TDP-43^{A315T} mice. By integrating histological and molecular findings across disease stages with emerging evidence of central metabolic dysregulation, our results provide a preliminary framework for understanding how peripheral and central alterations converge to shape systemic metabolic dysfunction in ALS. These observations underscore the importance of considering sex as a biological variable in biomarker development and in the design of nutritional therapeutic strategies.

While the present study is limited by its reliance on a single ALS mouse model and does not directly address causality between adipose tissue pathology and neurodegeneration, it highlights the relevance of the adipose-brain axis in ALS pathophysiology. In addition, although significant alterations in adipose tissue remodeling, leptin signaling, and metabolic parameters were identified, the molecular mechanisms underlying these changes were not directly investigated. Another limitation is the relatively small sample size, which may reduce the statistical power to detect subtle effects. Moreover, these findings have not yet been validated in human samples; therefore, their translational relevance should be interpreted with caution.

From a translational perspective, adipose tissue biomarkers and metabolic profiling may help identify sex-specific alterations associated with disease progression and treatment response. Furthermore, the adipose-brain axis may represent a potential therapeutic target for interventions aimed at improving energy homeostasis and mitigating metabolic dysfunction in ALS. Ongoing studies in our group examining additional adipose depots are expected to provide a more comprehensive view of systemic adipose tissue remodeling in ALS. Integrating information from multiple adipose depots may help define sex-specific metabolic signatures associated with distinct disease phenotypes, potentially supporting more personalized therapeutic and nutritional strategies for male and female patients. Future studies should aim to elucidate the molecular mechanisms underlying this bidirectional crosstalk, assess its translational relevance in human disease, and determine whether targeting these pathways can modify disease progression or metabolic dysfunction. Validation in clinical cohorts, together with studies in additional ALS models, such as SOD1 mice, will be essential to determine whether the sex-specific alterations in adipose tissue remodeling, leptin signaling, and metabolic regulation identified in the present study represent robust and clinically relevant features of ALS pathology.

Declarations

Ethics approval and consent to participate

All animal procedures were performed in accordance with the Animal Ethics Committee of the Hospital Nacional de Parapléjicos (Approval No 36OH/2019) (Spain) in accordance with the European Communities Council Directive (86/609/EEC) for the Care and Use of Animals for Scientific Purposes.

Consent for publication

All authors have read and agreed to the published version of the manuscript.

Competing interests

The authors declare that they have no competing interests.

Funding

The project leading to these results is funded by “la Caixa” Banking Foundation and co-funded by Fundación Luzón under the project code (LCF/PR/HR19/52160016), Spain.

Author Contribution

C-BC, A-FD collected the tissues; C-BC, E-DM performed histological data analysis; C-BC, C-FM performed statistical analysis and prepared the figures. C-FM conceived and designed the study. C-BC, C-FM drafted the manuscript. All authors critically reviewed the manuscript for intellectual content. All authors have read and agreed to the published version of the manuscript.

Acknowledgement

The authors would like to thank the Surgery Unit of the Hospital Nacional de Parapléjicos, Toledo (Spain) for their excellent technical support. In addition, Cristina Benito-Casado is supported by a PhD Fellowship from the Consejería de Educación, Ciencia y Universidades Comunidad de Madrid (PIPF-2023/SAL-GL-29613).

Data Availability

The datasets used and/or analysed during the current study are available from the corresponding author on reasonable request.

References

1. Ahmed RM, Phan K, Highton-williamson E, Strikwerda-brown C, Caga J, Ramsey E, Zoing M, Devenney E, Kim WS, Hodges JR, Piguet O, Halliday GM, Kiernan MC (2019) Eating peptides: Biomarkers of neurodegeneration in amyotrophic lateral sclerosis and frontotemporal dementia. Ann Clin Transl Neurol 6(3):486. https://doi.org/10.1002/acn3.721
2. Al-Khayri JM, Ravindran M, Banadka A, Vandana CD, Priya K, Nagella P, Kukkemane K (2024) Amyotrophic lateral sclerosis: Insights and new prospects in disease pathophysiology, biomarkers and therapies. Pharmaceuticals (Basel Switzerland) 17(10):1391. https://doi.org/10.3390/ph17101391

3. Becerril S, Rodríguez A, Catalán V, Ramírez B, Mentxaka A, Neira G, Gómez-Ambrosi J, Frühbeck G (2022) Sex- and age-dependent changes in the adiponectin/leptin ratio in experimental diet-induced obesity in mice. Nutrients 15(1):73. https://doi.org/10.3390/nu15010073
4. Benito-Casado C, Durán-Mateos E, Ferrer-Donato Á, García GB, Domínguez-Rubio R, Povedano M, Fernandez-Martos CM (2025))a. White adipose tissue undergoes pathological dysfunction in the TDP-43A315T mouse model of amyotrophic lateral sclerosis (ALS). Acta Neuropathol Commun 13(1):213. https://doi.org/10.1186/s40478-025-02130-9
5. Benito-Casado C, Ferrer-Donato Á, Fernandez-Martos CM (2025) b. Sex-specific hypothalamic axis disruption in the rNLS8 mouse model of amyotrophic lateral sclerosis (ALS). 10.1101/2025.07.23.666305v1. PREPRINT)https://www.biorxiv.org/content/
6. Cancello R, Tordjman J, Poitou C, Guilhem G, Bouillot JL, Hugol D, Coussieu C, Basdevant A, Hen B, Bedossa A, Guerre-Millo P, M., Clément K (2006) Increased infiltration of macrophages in omental adipose tissue is associated with marked hepatic lesions in morbid human obesity. Diabetes 55(6):1554–1561. https://doi.org/10.2337/db06-0133
7. Caron A, Lee S, Elmquist JK, Gautron L (2018) Leptin and brain-adipose crosstalks. Nat Rev Neurosci 19(3):153–165. https://doi.org/10.1038/nrn.2018.7
8. Chavakis T, Alexaki VI, Ferrante AW (2023) Macrophage function in adipose tissue homeostasis and metabolic inflammation. Nat Immunol 24(5):757–766. https://doi.org/10.1038/s41590-023-01479-0
9. Chen-Plotkin AS, Lee VM, -., Trojanowski JQ (2010) TAR DNA-binding protein 43 in neurodegenerative disease. Nat Reviews Neurol 6(4):211–220. https://doi.org/10.1038/nrneurol.2010.18
10. Cinti S, Mitchell G, Barbatelli G, Murano I, Ceresi E, Faloia E, Wang S, Fortier M, Greenberg AS, Obin MS (2005) Adipocyte death defines macrophage localization and function in adipose tissue of obese mice and humans. J Lipid Res 46(11):2347–2355. https://doi.org/10.1194/jlr.M500294-JLR200
11. Evans MC, Lord RA, Anderson GM (2021) Multiple leptin signalling pathways in the control of metabolism and fertility: A means to different ends? Int J Mol Sci 22(17):9210. https://doi.org/10.3390/ijms22179210
12. Fernandez CM, del Arco A, Gallardo N, Aguado L, Rodriguez M, Ros M, Carrascosa JM, Andres A, Arribas C (2010) S-resistin inhibits adipocyte differentiation and increases TNFalpha expression and secretion in 3T3-L1 cells. Biochim Biophys Acta 1803(10):1131–1141. https://doi.org/10.1016/j.bbamcr.2010.06.012
13. Ferrer-Donato A, Contreras A, Frago LM, Chowen JA, Fernandez-Martos CM (2021) Alterations in leptin signaling in amyotrophic lateral sclerosis (ALS). Int J Mol Sci 22(19):10305. 10.3390/ijms221910305
14. González-Fernández C, Fernández-Martos CM, Shields SD, Arenas E, Javier Rodríguez F (2014) Wnts are expressed in the spinal cord of adult mice and are differentially induced after injury. J Neurotrauma 31(6):565–581. https://doi.org/10.1089/neu.2013.3067

15. Grassano M, Moglia C, Palumbo F, Koumantakis E, Cugnasco P, Callegaro S, Canosa A, Manera U, Vasta R, De Mattei F, Matteoni E, Fuda G, Salamone P, Marchese G, Casale F, De Marchi F, Mazzini L, Mora G, Calvo A, Chio A (2024) Sex differences in amyotrophic lateral sclerosis survival and progression: A multidimensional analysis. Ann Neurol 96(1):159–169. https://doi.org/10.1002/ana.26933
16. Guilherme A, Tesz GJ, Guntur KVP, Czech MP (2009) Tumor necrosis factor-α induces caspase-mediated cleavage of peroxisome proliferator-activated receptor γ in adipocytes. J Biol Chem 284(25):17082–17091. https://doi.org/10.1074/jbc.M809042200
17. Hatzipetros T, Bogdanik LP, Tassinari VR, Kidd JD, Moreno AJ, Davis C, Osborne M, Austin A, Vieira FG, Lutz C, Perrin S (2014) C57BL/6J congenic prp-TDP43A315T mice develop progressive neurodegeneration in the myenteric plexus of the colon without exhibiting key features of ALS. Brain Res 1584:59–72. https://doi.org/10.1016/j.brainres.2013.10.013
18. Herz CT, Kiefer FW (2019) Adipose tissue browning in mice and humans. J Endocrinol 241(3):R97–R109. https://doi.org/10.1530/JOE-18-0598
19. Ikeda K, Yamada T (2020) UCP1 dependent and independent thermogenesis in brown and beige adipocytes. Front Endocrinol 11:498. https://doi.org/10.3389/fendo.2020.00498
20. Isidori AM, Strollo F, Morè M, Caprio M, Aversa A, Moretti C, Frajese G, Riondino G, Fabbri A (2000) Leptin and aging: Correlation with endocrine changes in male and female healthy adult populations of different body weights. J Clin Endocrinol Metabolism 85(5):1954–1962. https://doi.org/10.1210/jcem.85.5.6572
21. Ito Y, Daitoku H, Fukamizu A (2009) Foxo1 increases pro-inflammatory gene expression by inducing C/EBPbeta in TNF-alpha-treated adipocytes. Biochem Biophys Res Commun 378(2):290–295. https://doi.org/10.1016/j.bbrc.2008.11.043
22. Livak KJ, Schmittgen TD (2001) Analysis of relative gene expression data using real-time quantitative PCR and the 2(-delta delta C(T)) method. Methods (San Diego, Calif. 25(4):402–408. https://doi.org/10.1006/meth.2001.1262
23. Martin LJ, Wong M (2020) Skeletal muscle-restricted expression of human SOD1 in transgenic mice causes a fatal ALS-like syndrome. Front Neurol 11:592851. https://doi.org/10.3389/fneur.2020.592851
24. Morselli LL, Claflin KE, Cui H, Grobe JL (2018) Control of energy expenditure by AgRP neurons of the arcuate nucleus: Neurocircuitry, signaling pathways, and angiotensin. Curr Hypertens Rep 20(3):25. https://doi.org/10.1007/s11906-018-0824-8
25. Parlee SD, Lentz SI, Mori H, MacDougald OA (2014) Quantifying size and number of adipocytes in adipose tissue. Methods Enzymol 537:93–122. https://doi.org/10.1016/B978-0-12-411619-1.00006-9
26. Picher-Martel V, Boutej H, Vezina A, Cordeau P, Kaneb H, Julien J, Genge A, Dupre N, Kriz J (2023) Distinct plasma immune profile in ALS implicates sTNFR-II in pAMPK/leptin homeostasis. Int J Mol Sci 24(6):5065. 10.3390/ijms24065065

27. Rodriguez A, Ferrer-Donato A, Sesena S, Fernández P, Aranda A, Fernandez-Martos CM (2021) Repeated exposure to ozone produces changes in metabolic disturbances present in the TDP-43A315T transgenic model of amyotrophic lateral sclerosis. Diagn Pathology: Open Access, 1–7. https://www.omicsonline.org/open-access/repeated-exposure-to-ozone-produces-changes-in-metabolic-disturbances-present-in-the-tdp43a315t-transgenic-model-of-amyotrophic-la-117770.html
28. Rodríguez-Sánchez S, Valiente N, Seseña S, Cabrera-Pinto M, Rodríguez A, Aranda A, Palop L, Fernández-Martos CM (2022) Ozone modified hypothalamic signaling enhancing thermogenesis in the TDP-43A315T transgenic model of amyotrophic lateral sclerosis. Sci Rep 12(1):20814. https://doi.org/10.1038/s41598-022-25033-4
29. Rosina M, Scaricamazza S, Fenili G, Nesci V, Valle C, Ferri A, Paronetto MP (2025) Hidden players in the metabolic vulnerabilities of amyotrophic lateral sclerosis. Trends Endocrinol Metab. https://doi.org/10.1016/j.tem.2025.02.004
30. Sabaratnam R (2025) The endocrine effects of leptin on energy metabolism. Nat Rev Endocrinol 21(8):461. https://doi.org/10.1038/s41574-025-01135-7
31. Steyn FJ, Ioannides ZA, van Eijk RPA, Heggie S, Thorpe KA, Ceslis A, Heshmat S, Henders AK, Wray NR, van den Berg LH, Henderson RD, McCombe PA, Ngo ST (2018) Hypermetabolism in ALS is associated with greater functional decline and shorter survival. J Neurol Neurosurg Psychiatry 89(10):1016–1023. https://doi.org/10.1136/jnnp-2017-317887
32. Sun K, Tordjman J, Clément K, Scherer PE (2013) Fibrosis and adipose tissue dysfunction. Cell Metabol 18(4):470–477. https://doi.org/10.1016/j.cmet.2013.06.016
33. Thompson D, Williams C, Tosolini AP, Gilthorpe J, Schiavo G, Fisher EMC, Cunningham TJ (2025) Metabolic alterations in the absence of a detectable neuromuscular phenotype in novel genomically. 10.1101/2025.05.01.650597v1. humanised SOD1A4V micehttps://www.biorxiv.org/content/
34. Walker AK, Spiller KJ, Ge G, Zheng A, Xu Y, Zhou M, Tripathy K, Kwong LK, Trojanowski JQ, Lee VM, - (2015) Functional recovery in new mouse models of ALS/FTLD after clearance of pathological cytoplasmic TDP-43. Acta Neuropathol 130(5):643–660. https://doi.org/10.1007/s00401-015-1460-x
35. Wegorzewska I, Bell S, Cairns NJ, Miller TM, Baloh RH (2009) TDP-43 mutant transgenic mice develop features of ALS and frontotemporal lobar degeneration. Proc Natl Acad Sci USA 106(44):18809–18814. https://doi.org/10.1073/pnas.0908767106
36. Zwick RK, Guerrero-Juarez CF, Horsley V, Plikus MV (2018) Anatomical, physiological, and functional diversity of adipose tissue. Cell Metabol 27(1):68–83. https://doi.org/10.1016/j.cmet.2017.12.002

Figures

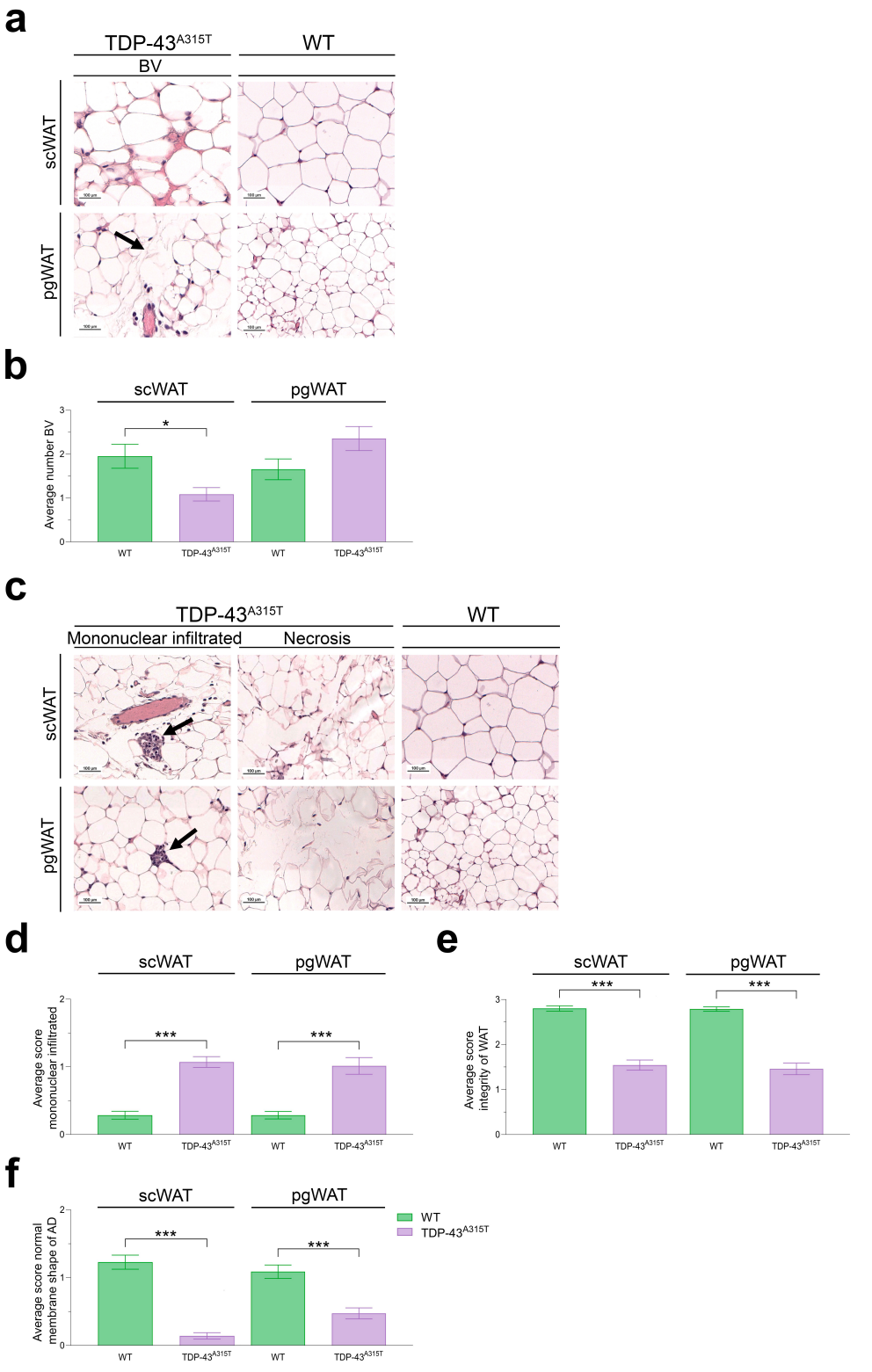


Figure 1

Histological H&E analysis of scWAT and pgWAT at 42 d of age of female TDP-43^{A315T} mice. (a) Representative images of BV (section bar = 100 μm, 20× magnification). **(b)** Semi-quantitative analysis of BV. **(c)** Representative images of mononuclear cell infiltrate (section bar = 100 μm, 10× magnification) and necrosis markers (section bar = 100 μm, 10× magnification for scWAT and 20× magnification for pgWAT). **(d)** Semi-quantitative analysis of mononuclear cell infiltrate, **(e)** WAT integrity and **(f)** normal

adipocyte membrane shape. WT representative images have section bar = 100 μm and 20× magnification for scWAT and 10× magnification for pgWAT. *$p < 0.05$, **$p < 0.01$, ***$p < 0.001$. Abbreviations: H&E, hematoxylin and eosin; scWAT, subcutaneous white adipose tissue; pgWAT, perigonadal white adipose tissue; 42 d, 42 days; BV: blood vessels; WAT, white adipose tissue; WT, wild-type.

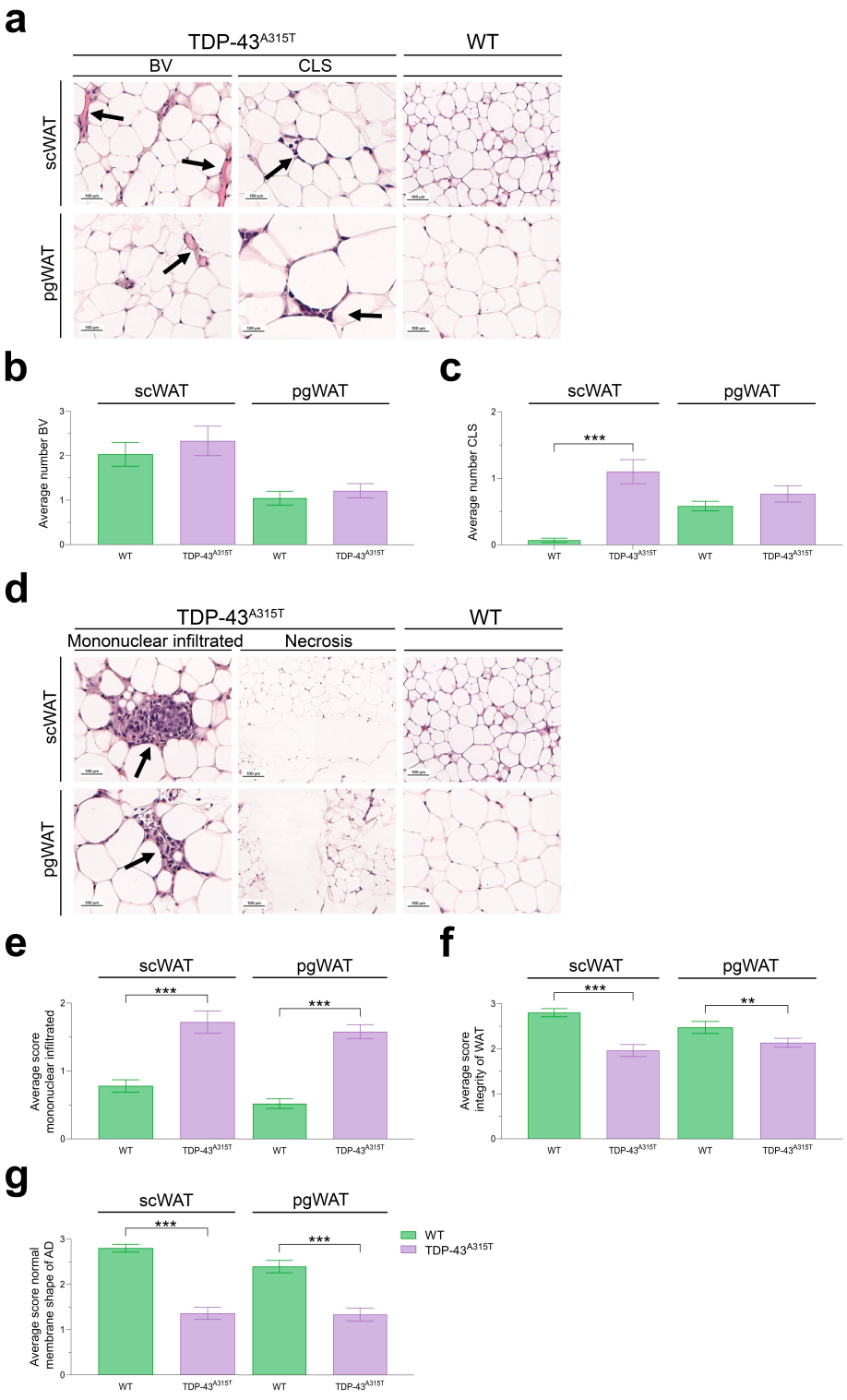


Figure 2

Histological H&E analysis of scWAT and pgWAT at 60 d of age of female TDP-43^{A315T} mice. (a) Representative images of BV and CLSs (section bar = 100 μm, 20× magnification). **(b)** Semi-quantitative analysis of BV and **(c)** CLSs. **(d)** Representative images of mononuclear cell infiltrate (section bar = 100 μm, 10× magnification for scWAT and 20× magnification for pgWAT) and necrosis markers (section bar = 100 μm, 10× magnification). **(e)** Semi-quantitative analysis of mononuclear cell infiltrate, **(f)** WAT integrity and **(g)** normal adipocyte membrane shape. WT representative images have section bar = 100 μm and 10× magnification for scWAT and 20× magnification for pgWAT. $^{**}p < 0.01$, $^{***}p < 0.001$. Abbreviations: H&E, hematoxylin and eosin; scWAT, subcutaneous white adipose tissue; pgWAT, perigonadal white adipose tissue; 60 d, 60 days; BV: blood vessels; CLSs, crown-like structures; WAT, white adipose tissue; WT, wild-type.

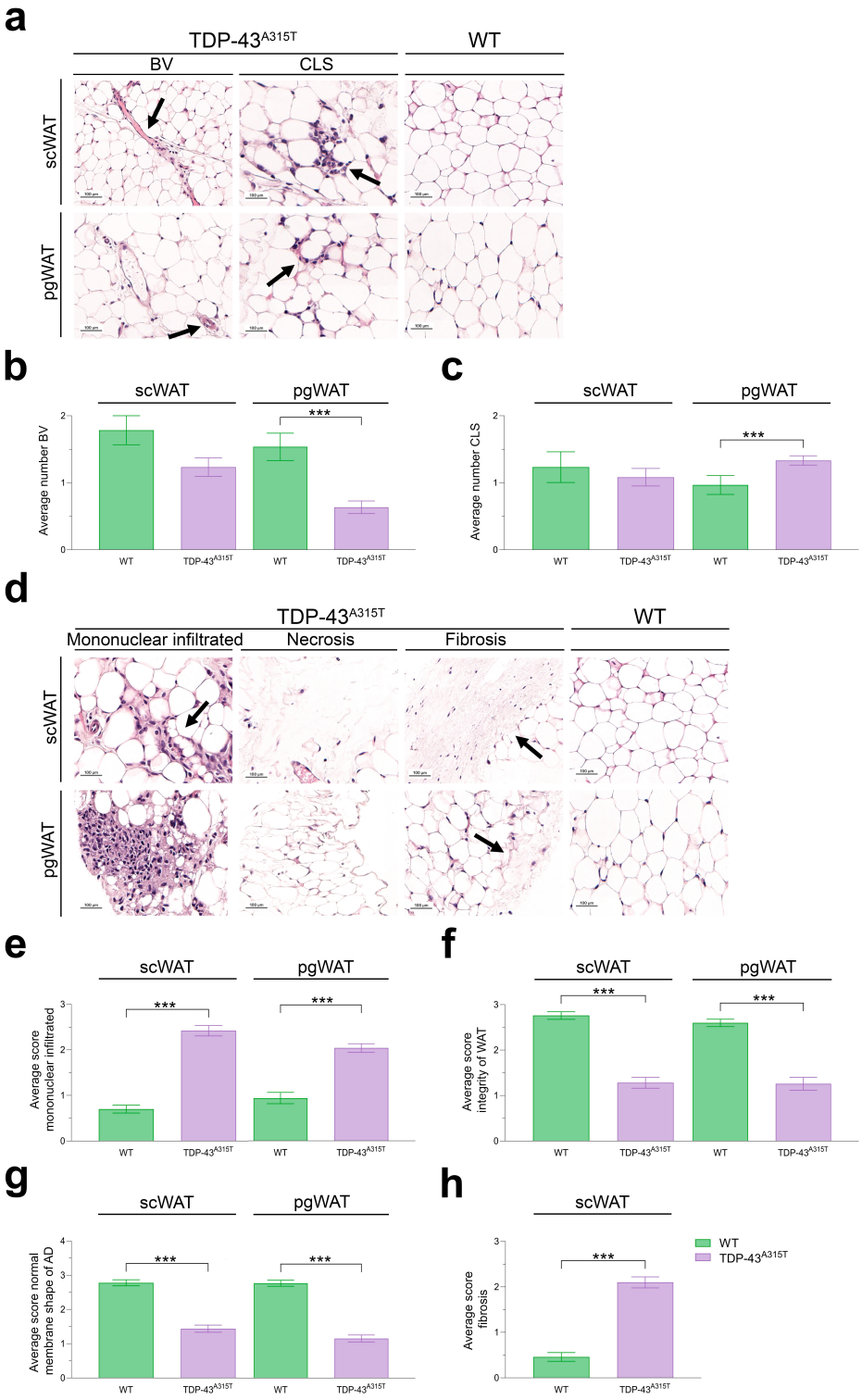


Figure 3

Histological H&E analysis of scWAT and pgWAT at 95 d of age of female TDP-43^{A315T} mice. (a) Representative images of BV (section bar = 100 µm, 10× magnification for scWAT and 20× magnification for pgWAT) and CLSs (section bar = 100 µm, 20× magnification for scWAT and 10× magnification for pgWAT). **(b)** Semi-quantitative analysis of BV and **(c)** CLSs. **(d)** Representative images of mononuclear cell infiltrate (section bar = 100 µm, 20× magnification), necrosis markers (section bar = 100 µm, 20×

magnification for scWAT and 10× magnification for pgWAT) and fibrosis (section bar = 100 µm, 20× magnification). **(e)** Semi-quantitative analysis of mononuclear cell infiltrate, **(f)** WAT integrity, **(g)** normal adipocyte membrane shape and **(h)** fibrosis. WT representative images have section bar = 100 µm and 10× magnification for scWAT and 20× magnification for pgWAT. ***$p < 0.001$. Abbreviations: H&E, hematoxylin and eosin; scWAT, subcutaneous white adipose tissue; pgWAT, perigonadal white adipose tissue; 95 d, 95 days; BV: blood vessels; CLSs, crown-like structures; WAT, white adipose tissue; WT, wild-type.

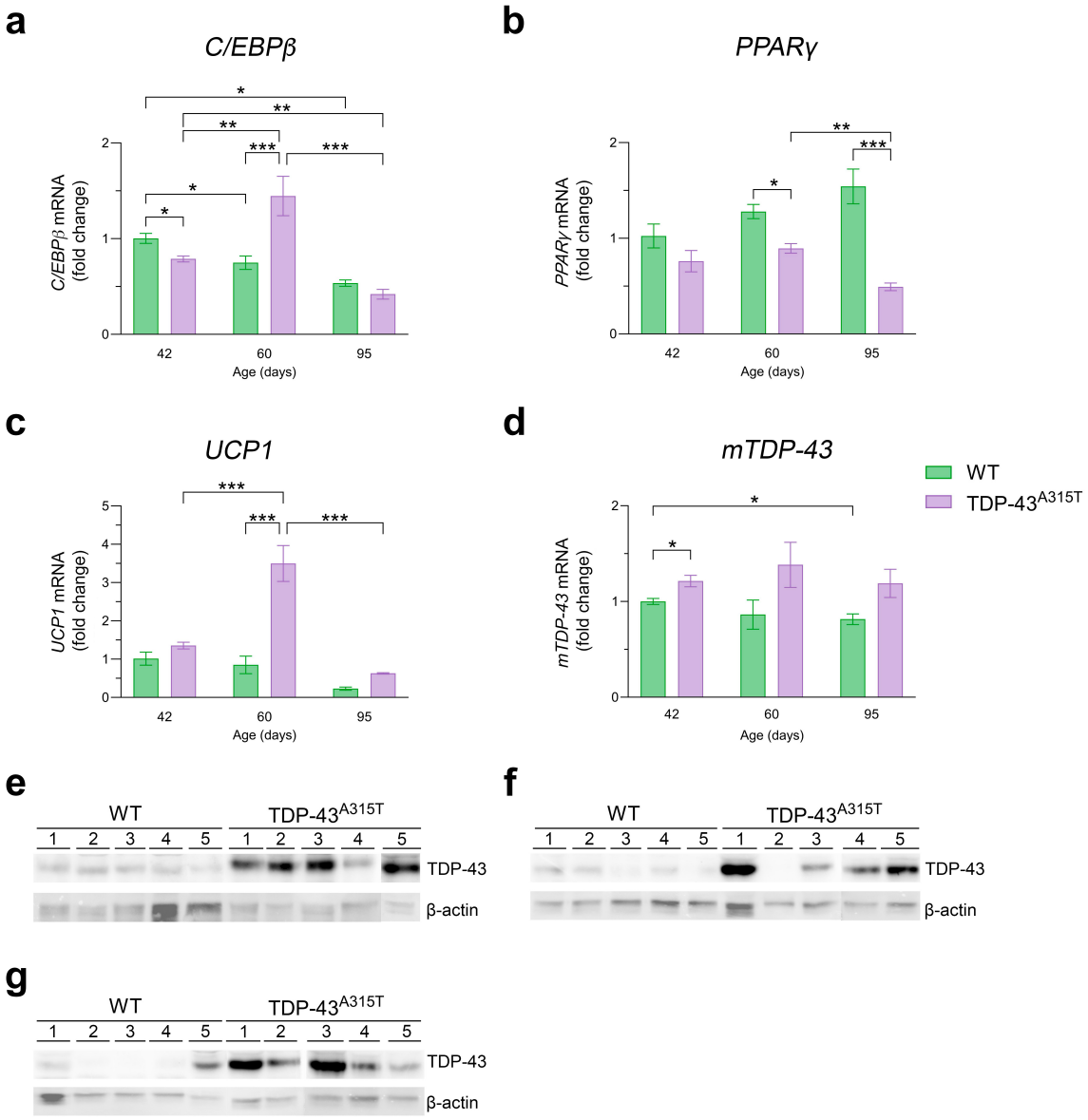


Figure 4

Differential expression of *C/EBPβ, PPARγ* and *UCP1* mRNA levels, and TDP-43 measured both at the mRNA level and by Western blot, in pgWAT of female TDP-43^{A315T} mice. (a) *C/EBPβ*, **(b)** *PPARγ*, **(c)** *UCP1* and **(d)** *mTDP-43* mRNA expression. Transcripts were assessed by RT-qPCR at 42 d, 60 d and 95 d. Values are expressed as mean ± SEM for each group. *$p < 0.05$, **$p < 0.01$, ***$p < 0.001$. **(e-g)** Representative Western blot images correspond to TDP-43 protein levels in pgWAT from female TDP-43^{A315T} mice at 42 d (**e**), 60 d (**f**), and 95 d (**g**) of age. The displayed lanes were not contiguous in the original gels; lanes were reordered solely for clarity of presentation, with no additional image manipulation. The original, unedited gels are provided in Supplementary Figure 1. Abbreviations: C/EBPβ, CCAAT/enhancer-binding protein beta; PPARγ, peroxisome proliferator-activated receptor gamma; UCP1, uncoupling protein 1; TDP-43, TAR DNA-binding protein 43; pgWAT, perigonadal white adipose tissue; 42 d, 42 days; 60 d, 60 days; 95 d, 95 days; SEM, standard error of the mean.

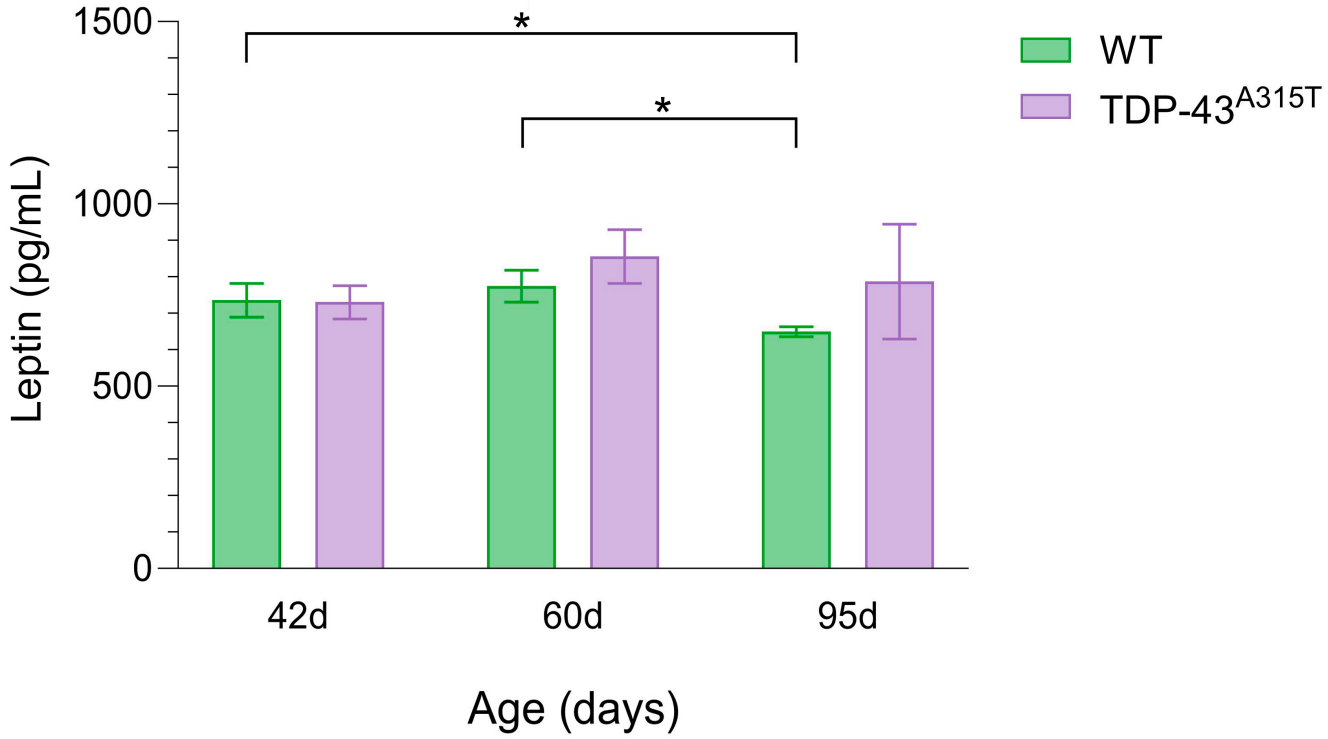


Figure 5

Plasma leptin levels in female TDP-43^{A315T} mice. Concentration of plasma leptin levels were measured in female WT and TDP-43^{A315T} mice at 42 d, 60 d and 95 d of age to evaluate age-dependent changes in circulating leptin levels. Values are expressed as mean ± SEM for each group. *$p < 0.05$. Abbreviations: 42 d, 42 days; 60 d, 60 days; 95 d, 95 days; SEM, standard error of the mean.

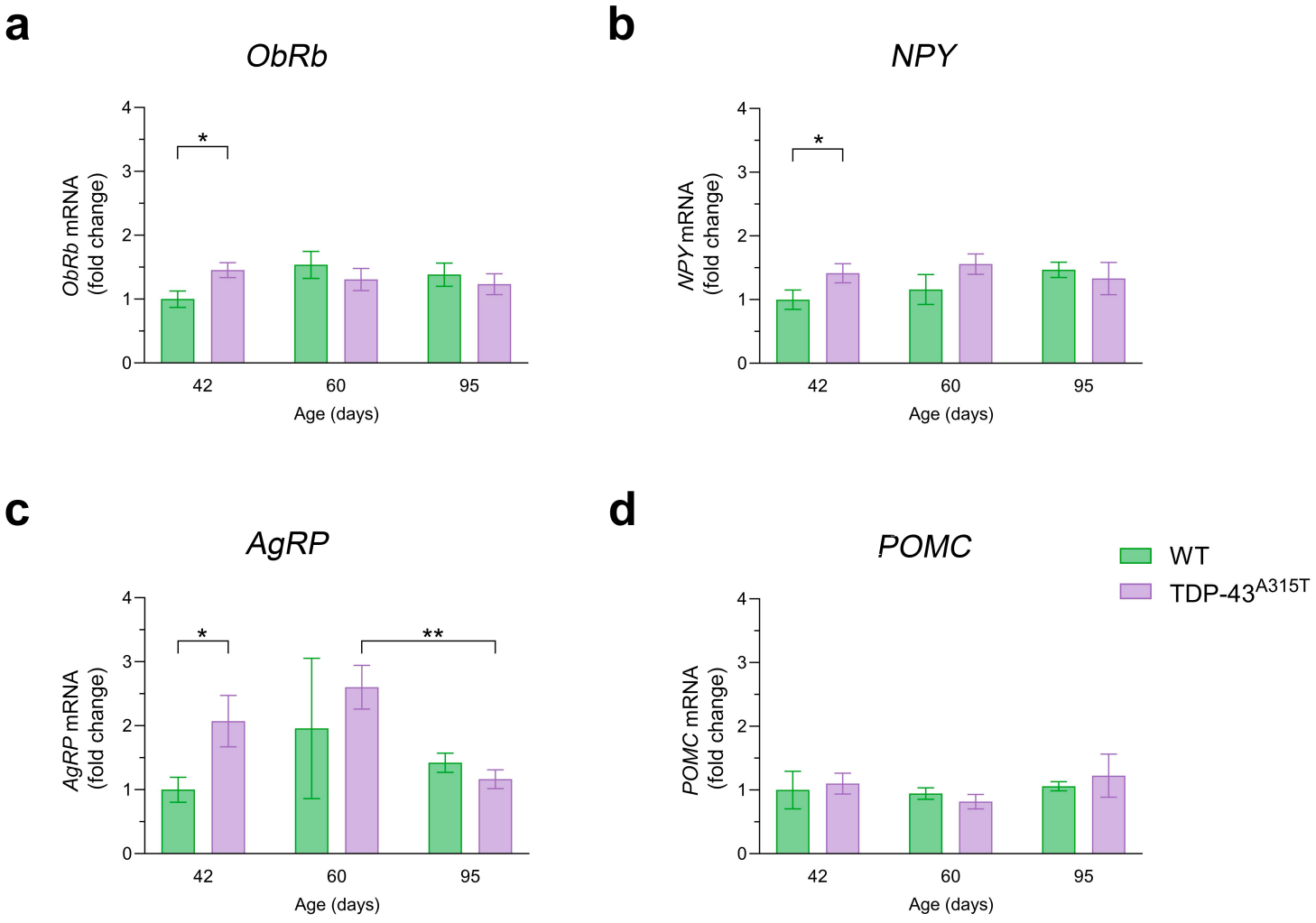


Figure 6

Differential expression of *ObRb, NPY, AgRP* and *POMC* mRNA levels in the hypothalamus of female TDP-43^{A315T} mice. (a) *ObRb*, **(b)** *NPY*, **(c)** *AgRP* and **(d)** *POMC* mRNA expression. Transcripts were assessed by RT-qPCR at 42 d, 60 d and 95 d of age. Values are expressed as mean ± SEM for each group. *$p < 0.05$, **$p < 0.01$. Abbreviations: ObRb, long form of the leptin receptor; NPY, Neuropeptide Y; AgRP, Agouti-related peptide; POMC, Pro-opiomelanocortin; 42 d, 42 days; 60 d, 60 days; 95 d, 95 days; SEM, standard error of the mean.

Supplementary Files

This is a list of supplementary files associated with this preprint. Click to download.

- Table1.docx
- SupplementaryFigure1.jpg